ACS OMEGA

Article

Cite This: ACS Omega 2019, 4, 13687−13695

http://pubs.acs.org/journal/acsodf

Membrane Surface-Enhanced Raman Spectroscopy for Cholesterol-Modified Lipid Systems: Effect of Gold Nanoparticle Size

Miftah Faried,[†] Keishi Suga,*[,†] Yukihiro Okamoto,[†] Kamyar Shameli,[‡] Mikio Miyake,[‡,§] and Hiroshi Umakoshi*[,†]

[†]Division of Chemical Engineering, Graduate School of Engineering Science, Osaka University, 1-3 Machikaneyama-cho, Toyonaka, Osaka 560-8531, Japan

[‡]Department of Environment and Green Technology, Malaysia−Japan International Institute of Technology, Universiti Teknologi Malaysia, Jalan Sultan Yahya Petra, Kuala Lumpur 54100, Malaysia

[§]School of Materials Science, Japan Advanced Institute of Science and Technology, 1-1 Asahidai, Nomi, Ishikawa 923-1292, Japan

Supporting Information

ABSTRACT: A gold nanoparticle (AuNP) has a localized surface plasmon resonance peak depending on its size, which is often utilized for surface-enhanced Raman scattering (SERS). To obtain information on the cholesterol (Chol)-incorporated lipid membranes by SERS, AuNPs (5, 100 nm) were first functionalized by 1-octanethiol and then modified by lipids (AuNP@lipid). In membrane surface-enhanced Raman spectroscopy (MSERS), both signals from 1,2-dioleoyl-*sn*-glycero-3-phosphocholine (DOPC) and Chol molecules were enhanced, depending on preparation conditions (size of AuNPs and lipid/AuNP ratio). The enhancement factors (EFs) were calculated to estimate the efficiency of AuNPs on Raman enhancement. The size of $AuNP_{100nm}$@lipid was 152.0 ± 12.8 nm, which showed an surface enhancement Raman spectrum with an EF_{2850} value of 111 ± 9. The size of $AuNP_{5nm}$@lipid prepared with a lipid/AuNP ratio of 1.38×10^4 (lipid molecule/particle) was 275.3 ± 20.2 nm, which showed the highest enhancement with an EF_{2850} value of 131 ± 21. On the basis of fluorescent probe analyses, the membrane fluidity and polarity of AuNP@lipid were almost similar to DOPC/Chol liposome, indicating an intact membrane of DOPC/Chol after modification with AuNPs. Finally, the membrane properties of AuNP@lipid systems were also discussed on the basis of the obtained MSERS signals.

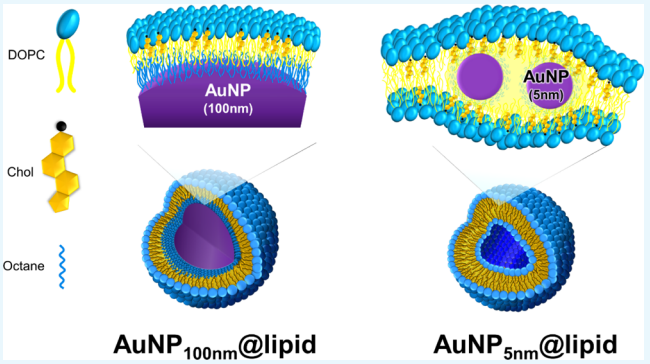

INTRODUCTION

Metal nanomaterials, such as gold nanoparticles (AuNPs), have attracted attention in the analysis of biological molecules. Depending on the sizes, the AuNPs show a localized surface plasmon resonance peak,[1] which can be applied in sensor development and surface-enhanced Raman scattering (SERS).[2−4] In addition, because the surface of AuNPs can be modified by various types of molecules, AuNPs are widely utilized in drug delivery systems, imaging, sensors, and medical engineering.[5−8] In biological systems, a self-organized lipid membrane has several important roles such as controlling the structure of membrane protein, transporting molecules across the membrane, and signal transduction using mediators. To better understand such emergent functions that have arisen at the membrane interface,[9,10] localized molecular behavior and lipid membrane property studies are necessary. However, the investigation of the fundamental properties of lipid membranes based on lipid information is challenging. Thus, methods based on SERS are applied for membrane studies, wherein a Raman probe, which is localized in the membrane and emits strong signals when excited by a laser, is usually employed to ensure lipid membranes. Carbonate-capped AuNPs were utilized as artificial ion transporters across biological membranes.[11] Owing to the surface properties, the synthetic nanoparticles (NPs) can interact with lipid membranes.[12,13] The AuNPs were utilized to determine the surface charge of lipid membranes.[14] SERS techniques are also applied to living cell membrane systems.[15] Raman signals enable the identification of the structural information of lipid molecules in the membrane.[16,17] In addition, metal nanostructures have discovered the hot spot which produced strong Raman signals.[18] Thus, the location of NPs must be controlled to gain in situ information from the enhanced Raman spectrum.

There has been significant interest in molecular behaviors of membrane components such as cholesterol (Chol) and sphingomyelin. Direct spectroscopy measurements, such as

Received: April 15, 2019
Accepted: August 5, 2019
Published: August 19, 2019

DOI: 10.1021/acsomega.9b01073
ACS Omega 2019, 4, 13687−13695

Raman, infrared, nuclear magnetic resonance, calorimetry, and so forth, have been employed to understand self-assembly behaviors of membrane lipids. However, signal intensities are sometimes problematic for quantitative analysis. The use of fluorescence probe is also a reliable method to study membrane properties, such as 1,6-diphenyl-1,3,5-hexatriene (DPH) for membrane fluidity ($1/P$) and 6-lauroyl-2-dimethylaminonaphthalene (Laurdan) for membrane polarity (GP_{340}). These methods are powerful to wheel the lipid membrane studies until now; however, a concern is that the probe signal is indirect. Although an SERS method requires membrane labeling with a plasmonic material (e.g., AuNP), it can directly reflect the molecular information of the target. Thus, the SERS signals obtained from a lipid membrane could provide spontaneous information about lipids (molecular conformation and localization). Table 1 describes some previous studies on inner membrane analysis. Zhang and Granick analyzed the lateral lipid diffusion in the inner and outer leaflets in planar-supported lipid bilayers and suggested that the component in the inner leaflet typically diffused slowly.[19] Murzyn et al. analyzed an inner bacterial membrane composed of phosphatidylethanolamine (PE) and phosphatidylglycerol (PG) and built a computer model showing the interactions of the bilayer interfacial regions via intermolecular hydrogen bond and water bridges, revealing that PE and PG strongly interacted in the bilayer.[20] In addition, an intensive inner lipid study on Chol was performed through various methods.[21−23] However, nanodomains could be visualized with the advanced microscopy equipment.[24]

Table 1. Summary of Inner Membrane Studies Reported in Literature

method of study	amphiphilic molecules	refs
inner leaflet diffusion	DLPC, DMPE	19
Chol inner surface lipid	DPPC, egg PC (conc. 55 ± 5 mM)	48
inner bacterial membrane via MD simulation	POPE, POPG	20
mitochondrial inner membrane with mathematical model	lipid hydroperoxides	49

Typically, the thickness of a lipid bilayer vesicle is approximately 4−6 nm. The hydrophilic NPs are located on the outer leaflet of liposomes,[25] whereas the hydrophobic NPs are internalized in the lipid membranes depending on the particle size.[26] In multilayer membranes, synthesized NPs (diameter: ca. 5 nm) can be embedded into bilayers.[27,28] Hydrophobic AuNPs can also be embedded into a lipid bilayer,[29] suggesting that the SERS technique can be applied to detect hydrophobic materials existing in the lipid membranes. Because a membrane of Chol-enriched domains (liquid-ordered phase, composed with saturated lipids and sphingolipids) tends to be thicker than a fluid membrane (without Chol), there might be disadvantages in utilizing large-sized AuNPs.

In our previous study, $AuNP_{100nm}$ was utilized to study self-assembled phospholipid membranes ($AuNP_{100nm}$@lipid), and a method to obtain highly sensitive lipid membrane information using $AuNP_{100nm}$@lipid was developed, known as membrane surface-enhanced Raman spectroscopy (MSERS).[30] Using the enhancement factor (EF) as the indicator to determine the efficiency of Raman enhancement for a target molecule,[31] the membrane thickness was found to be possibly relevant to Raman enhancement because a hot spot can occur at the contact surface between the AuNPs. The enhancement mechanism for $AuNP_{100nm}$ systems is as follows: the 100 nm AuNPs served as a core around which lipids were coated. The sonication treatment (60 min in a sonication bath) decreased the aggregation of $AuNP_{100nm}$@lipid particles. For long periods of incubation, some $AuNP_{100nm}$@lipid particles were aggregated with each other. Simultaneously, the lipid membranes were sandwiched between the AuNPs (hot spot). However, the $AuNP_{100nm}$@lipid system has the following disadvantages: (1) thicker membrane (C−H chains longer than C18) shows smaller enhancement because enhancement depends on the distance between the lipid-coated AuNPs, and (2) the charged membrane did not cause SERS because the electrostatic repulsion between the lipid-coated AuNPs increases the distance between them. The distance between the two AuNPs is critical for the SERS intensity.[32,33]

In this work, we aim to develop a SERS-based characterization for the lipid membrane systems, particularly to compare the effect on AuNP size on SERS performances. Herein, two types of AuNPs were employed: the systems utilizing $AuNP_{100nm}$[30] and $AuNP_{5nm}$. The prepared $AuNP_{5nm}$@lipid and $AuNP_{100nm}$@lipid were characterized on the basis of conventional fluorescent probe methods and of SERS analysis. Lipid membranes were composed of 1,2-dioleoyl-*sn*-glycero-3-phosphocholine (DOPC)/Chol = (60/40). A side-by-side comparison of membrane properties was performed to ensure influences of AuNPs on lipid membranes. In addition, the phase state and membrane properties can be changed from liquid-disordered phase (DOPC-enrich) to liquid-ordered phase (Chol-enrich) depending on the Chol amount.[34,35] Then, the obtained results were discussed focusing on the influence of AuNPs, which could directly alter the membrane properties via AuNP−lipid interaction, and also an indirect influence, for example, the altered distribution (local concentration) of Chol because of the presence of AuNPs.

EXPERIMENTAL SECTION

Materials. DOPC was purchased from NOF Corporation (Tokyo, Japan). Chol and citrate-stabilized $AuNP_{100nm}$ (3.8×10^9 particles per mL) were purchased from Sigma-Aldrich (St. Louis, MO). 1-Octanethiol and other chemicals used in this study were purchased from Wako Pure Chemicals (Osaka, Japan) and used without further purification. Citrate-capped $AuNP_{5nm}$ was synthesized according to a previous report.[36] Briefly, a $HAuCl_4$ solution was mixed with an ice-cold $NaBH_4$ solution at 25 °C. The final concentrations of $HAuCl_4$, trisodium citrate, and $NaBH_4$ were 0.25, 1.25, and 1.25 mM, respectively. Cross-flow filtration was performed using a hollow tube (MicroKros Module, Spectrum Laboratories, Inc.) to concentrate AuNPs.

Preparation of AuNP@Lipid. The lipid composition used in this study was the mixture of DOPC/Chol (60/40). The $AuNP_{5nm}$@lipid samples were prepared by mixing 2 mL of 5 nm AuNP solution (total [Au] concentration of 0.14 mM), 3 mL of ethanol, and 10 μL of 1-octanethiol dissolved in chloroform (volume ratio: chloroform/1-octanethiol = 300/1). The mixture was stirred for 3 h at room temperature and then the solution was separated into two phases by incubating for 30 min. The bottom phase was transferred carefully to a round-bottomed flask. The solvent was removed by evaporation under vacuum condition. Afterward, the obtained 1-octanethiol-functionalized AuNPs were kept under high vacuum

DOI: 10.1021/acsomega.9b01073
ACS Omega 2019, 4, 13687−13695

overnight, thus completely removing the solvent. The $CHCl_3$ solution of lipids was applied to 1-octanethiol-functionalized AuNPs, and the solvents were removed by evaporation. The dried samples were hydrated with pure water. The lipid/$AuNP_{5nm}$ ratios used in this study were 1.38×10^4, 2.76×10^4, and 1.38×10^5 [lipid molecules/particle] (for details, see the Supporting Information). The $AuNP_{100nm}$@lipid samples were prepared according to the reported method.[30] These data were compared to discuss the difference of inner and outer membrane properties. Because the prepared AuNP@lipid samples included no precipitates of lipid, it is assumed that Chol was successfully incorporated into the lipid membrane. The concentration of DOPC was measured with an assay kit (Phospholipid C-Test; Wako Pure Chemical).[37]

Size Distributions of AuNP@Lipid. The hydrodynamic diameters and size distributions of the AuNP@lipid suspensions were determined at 25 °C using dynamic light scattering (DLS) [Zetasizer Nano (Malvern Instruments Ltd., Tokyo, Japan)]. The samples were measured as prepared (no pretreatment by filter), and no larger aggregates (size > 1 μm) were detected. The size distribution of $AuNP_{5nm}$ was determined by a scanning transmittance electron microscope (HD-2700B, Hitachi High-Technologies Corporation, Tokyo, Japan) at an accelerating voltage of 80 kV (Figure S1).

Raman Measurements of AuNP@Lipid. The Raman spectra of liposomes, $AuNP_{5nm}$@lipid, and $AuNP_{100nm}$@lipid were measured using a confocal Raman microscope (LabRAM HR-800, Horiba Ltd., Kyoto, Japan). A 532 nm YAG laser of 100 mW was used for excitation, and a 20× objective lens was used to focus the laser beam. The spatial resolution in the measurement was ca. 50 μm × 50 μm (x–y) and ca. 5 μm (z). The prepared AuNP@lipid particles were small (diameter less than 1 μm). All the spectra reported here were measured with an accumulation time of 20 s, and each spectral data were accumulated five times. The measurements were carried out on a temperature-controlled Peltier plate, which kept the sample temperature at 25 °C. The background signal (water) was removed to obtain the actual Raman intensity of lipids (for details, see the Supporting Information).

Calculation of EF. To investigate the Raman signal, the EF value was calculated using the following equation

$$\mathrm{EF} = (I_{\mathrm{MSERS}}/C_{\mathrm{MSERS}})/(I_{\mathrm{liposome}}/C_{\mathrm{liposome}}) \quad (1)$$

where I_{MSERS} represents the Raman intensity obtained in AuNP@lipid, and C_{MSERS} represents the total concentration of lipid in AuNP@lipid. The I_{liposome} represents the Raman intensity obtained in DOPC/Chol (60/40) liposomes (no modification with AuNPs), wherein the total lipid concentration (=C_{liposome}) was 100 mM. The value of I/C indicates a normalized Raman intensity by applied lipid concentration. Raman spectrum measurements were conducted at least three times, and the average value of each peak intensity was employed to calculate EF.

Fluorescence Emission Spectra of Laurdan. Ten microliter of 100 μM Laurdan in ethanol was mixed with 12.5 μL of vesicle suspension, and the sample solution was diluted with water to a total volume of 1 mL. The molar ratio of total lipid/probe was 100/1. The sample solutions were incubated for 30 min at room temperature. Then, the fluorescence spectrum of Laurdan was recorded with an excitation wavelength of 340 nm, at emission wavelengths from 400 to 600 nm. The membrane polarity (GP_{340}) at different temperatures was determined from[35,38,39]

$$\mathrm{GP}_{340} = (I_{440} - I_{490})/(I_{440} + I_{490}) \quad (2)$$

where I_{440} and I_{490} are the emission intensities of Laurdan at 440 and 490 nm wavelengths, respectively.

Fluorescence Polarization Measurements. To measure membrane fluidity, 0.4 μL of 100 μM DPH ethanol solution was mixed with 12.5 μL of vesicle suspension. The sample solution was diluted with water to a total volume of 1 mL. The molar ratio of total lipid/probe was 250/1. Before fluorescence polarization measurements, the samples were incubated for 30 min at room temperature in the dark. After incubation, the fluorescence polarization of DPH was measured using a fluorescence spectrophotometer (FP-8500, Jasco, Tokyo, Japan) (Ex. = 360 nm, Em. = 430 nm). Fluorescence polarizers were set on the excitation and emission light pathways. With the emission polarizer angle of 0°, the fluorescence intensities obtained with the emission polarizer angle 0° and 90° were defined as $I_\perp$ and $I_\parallel$, respectively. With the emission polarizer angle of 90°, the fluorescence intensities obtained with the emission polarizer angle 0° and 90° were defined as $i_\perp$ and $i_\parallel$, respectively. The polarization (P) was then calculated using

$$P = (I_\parallel - GI_\perp)/(I_\parallel + GI_\perp) \quad (3)$$

where G (=$i_\perp/i_\parallel$) is the correction factor. Because polarization is inversely proportional to fluidity,[35,38] the membrane fluidity was evaluated by the reciprocal of polarization ($1/P$).

RESULTS AND DISCUSSION

Characterization of AuNP@Lipid Self-Assembly. $AuNP_{100nm}$@lipid and $AuNP_{5nm}$@lipid were prepared based on the same protocol. The hydrodynamic diameters of the self-assemblies were determined by DLS (Figure 1, Table 2). The

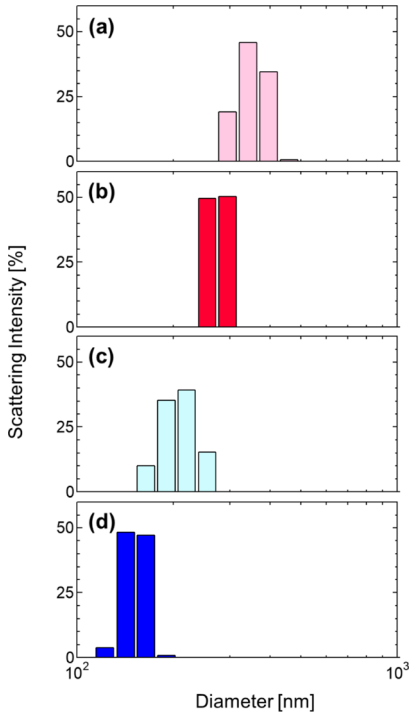

Figure 1. Size distributions of particles. (a) $AuNP_{5nm}$@lipid (just after prepared), (b) $AuNP_{5nm}$@lipid (after 60 min ultrasonication), (c) $AuNP_{100nm}$@lipid (just after prepared), and (d) $AuNP_{100nm}$@lipid (after 60 min ultrasonication). Lipid compositions were DOPC/Chol (60/40). All samples were measured at 25 °C.

DOI: 10.1021/acsomega.9b01073
ACS Omega 2019, 4, 13687−13695

Table 2. Particle Size of AuNP@Lipid

system	size [nm]
$AuNP_{5nm}$ [a]	4.8 [c]
$AuNP_{5nm}$@lipid	352.5 ± 37.4 [d]
$AuNP_{5nm}$@lipid + sonication (60 min)	275.3 ± 20.2 [d]
$AuNP_{100nm}$ [b]	115.5 ± 29.0 [b]
$AuNP_{100nm}$@lipid	209.4 ± 26.5 [d]
$AuNP_{100nm}$@lipid + sonication (60 min)	152.0 ± 12.8 [d]

[a]Synthesized based on the reported protocol.[36] [b]Purchased from Sigma-Aldrich and used as received (see Figure S1). [c]Size was determined by transmission electron microscopy (see Figure S1). [d]Size was determined by DLS.

average sizes of $AuNP_{100nm}$@lipid and $AuNP_{5nm}$@lipid were 209.4 ± 26.5 and 352.5 ± 37.4 nm, respectively. Ultrasound sonication (60 min) reduces the interparticle aggregates.[30] Consequently, the average sizes of $AuNP_{100nm}$@lipid and $AuNP_{5nm}$@lipid were decreased to 152.0 ± 12.8 and 275.3 ± 20.2 nm, respectively. In the following experiments, the ultrasound-treated AuNP@lipid samples were used.

MSERS Signals Obtained by $AuNP_{100nm}$@Lipid Systems. To clarify the modification model of the lipid membrane, the role of AuNPs in SERS from the lipid membrane was studied by selecting two AuNPs with different sizes [5 nm (small) and 100 nm (large)]. In a previous study, $AuNP_{100nm}$@lipid samples were prepared to analyze the surface region of the membrane leaflet.[30] Figure 2 shows MSERS of

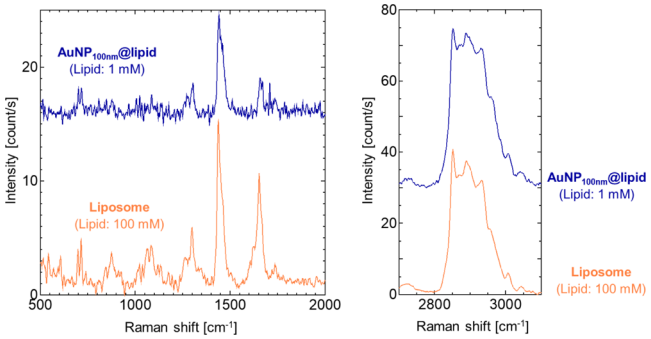

Figure 2. Raman spectra of $AuNP_{100nm}$@lipid (blue) and liposome (orange), obtained with total lipid concentrations of 1 and 100 mM, respectively. Lipid compositions were DOPC/Chol (60/40). All samples were measured at 25 °C. At least three reproducible spectra were obtained for each system. Raw spectral data are shown in the Supporting Information (Figure S2).

$AuNP_{100nm}$@lipid [total lipid: 1 mM (blue line)], compared to conventional liposome (100 mM, orange line). $AuNP_{100nm}$@lipid shows high Raman signals even in low lipid concentration (1 mM). The insertion of $AuNP_{100nm}$ successfully enhanced the Raman intensities both in the fingerprint (500−2000 cm^{-1}) and in the C−H stretching regions (2700−3100 cm^{-1}): peaks were clearly observed at 714 cm^{-1} [choline head group (DOPC)], 2852 cm^{-1} [symmetric stretching $-CH_2-$ (DOPC)], and 2872 cm^{-1} [asymmetric $-CH_2-$ (Chol)]. The enhancement in the fingerprint region was relatively weaker than that in the C−H stretching region. The enhancement of $AuNP_{100nm}$@lipid was further found to be sensitive to the membrane thickness,[30] suggesting that a hot spot can be formed in the thicker membrane region, that is, Chol-enriched domains. In the C−H stretching region (2700−3100 cm^{-1}), the peak at 2872 cm^{-1} was derived from Chol, while the peak at 2852 cm^{-1} originated from the hydrocarbon chain of the phospholipid (herein DOPC). The mechanism for the 100 nm AuNP systems was as follows (also see Suga et al.[30]): the 100 nm AuNP acts as a core, and the lipids were coated around the AuNPs. In our previous works, the sonication treatment (60 min in sonication bath) decreased the aggregation of $AuNP_{100nm}$@lipid particles. For longtime incubation, some $AuNP_{100nm}$@lipid particles were aggregated with each other. Simultaneously, the lipid membranes were sandwiched between the AuNPs (hot spot). Although the lipid membrane of $AuNP_{100nm}$@lipid system does "not" show a bilayer structure, the membrane properties are quite similar to the liposome systems.

MSERS Signals Obtained from $AuNP_{5nm}$@Lipid Systems. $AuNP_{5nm}$@lipid systems are expected to enhance the inner membrane region because of the embedding small AuNPs. In a similar way, to prepare $AuNP_{100nm}$@lipid systems, the $AuNP_{(5nm)}$ was first modified with 1-octanethiol as the hydrophobic dispersing agent, which could then be embedded into the lipid bilayers. Small AuNPs could be located between the bilayer membrane, owing to their small size (approximately 5 nm), and the small space between the bilayer leaflet. In theory, NPs (diameter, ca. 5 nm) can be inserted into lipid bilayers.[26] The synthesized small $AuNP_{5nm}$ was implemented in DOPC/Chol (60/40) membranes. Figure 3 shows that

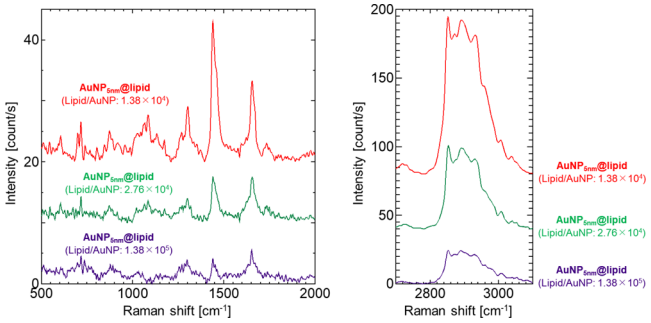

Figure 3. Raman spectra of $AuNP_{5nm}$@lipid, with different lipid/AuNP ratios: red, lipid/AuNP = 1.38 × 10^4; green, lipid/AuNP = 2.76 × 10^4; and purple, lipid/AuNP = 1.38 × 10^5. Lipid compositions were DOPC/Chol (60/40). All samples were measured at 25 °C. At least three reproducible spectra were obtained for each system. Raw spectral data are shown in the Supporting Information (Figure S2).

several lipid/AuNP ratios were tested for MSERS: lipid/AuNP ratios such as 1.38 × 10^4 [total lipid: 0.5 mM (red line)], 2.76 × 10^4 [total lipid: 1.0 mM (green line)], and 1.38 × 10^5 [total lipid: 5.0 mM (purple line)]. The embedding of $AuNP_{5nm}$ was entrapped in the hydrophobic area of the bilayer, thereby enabling the enhancement of Raman signals at the inner membrane region. This indicates that the MSERS signals obtained from $AuNP_{5nm}$@lipid systems are sensitive to the lipid/AuNP ratio.

Herein, it is assumed that a liposome (unilamellar vesicle) with a diameter of 300 nm is composed of ∼100 000 units of lipid. When the prepared AuNP@lipid is composed of unilamellar vesicle with a diameter of ∼280 nm (estimated by DLS), with lipid/AuNP ratio = 1.38 × 10^4, hopefully several NPs exist in assembly. When the lipid/AuNP ratio = 1.38 × 10^5, only one (or less than 1) AuNP exists in assembly, and the gap formation within the assembly could be difficult. Thus, a larger lipid/AuNP ratio would increase the possibility of the

DOI: 10.1021/acsomega.9b01073
ACS Omega 2019, 4, 13687−13695

gap between AuNPs in a vesicular envelope. The occurrences of hot spots increase as more AuNPs occur in the membrane and the lipid/AuNP ratio is reduced. Focusing on $AuNP_{5nm}$@lipid with a lipid/AuNP ratio of 1.38×10^4, $AuNP_{5nm}$@lipid showed several peaks both in the fingerprint and the C−H stretching regions compared to that of $AuNP_{100nm}$@lipid. These enhanced signals were due to the hot spot from the AuNP.[40] However, a low ratio of lipid/AuNP was observed at the highest Raman signal, likely because of the closer distances between embedded AuNPs to produce the hot spot. In addition, it was concluded that $AuNP_{5nm}$ was inserted into the vesicle owing to the hydrophobic interaction between the AuNP and the lipid bilayers. Therefore, MSERS signals showed clearer peaks, notably at the fingerprint area, which has several hydrophobic parts of lipid.

Comparison of EF for AuNP@Lipid Systems. The analysis of Raman spectra is required after embedding small AuNPs into the lipid bilayer. The EF is necessary in SERS study to determine and understand the efficiency of Raman enhancement by using small AuNPs. The SERS intensity is relevant to the distance between the target molecule and NP and the number of target molecules associated with NPs.[41] To simplify, eq 1 can be employed to estimate the efficiency of Raman enhancement by modifying with alkanethiol-functionalized AuNPs.[30] Here, Raman spectroscopy measurements were conducted for the samples. Total lipid concentrations for $AuNP_{100nm}$@lipid and $AuNP_{100nm}$@lipid systems were 0.5 and 1 mM. Thus, the EF values can be indicators to optimize the preparation of AuNP@lipid systems. $AuNP_{5nm}$@lipid has greatly contributed to the membrane interior analysis, which enables AuNPs to locate into the nanodomain lipid bilayer.[42] The DOPC and Chol peaks packed in the interior membrane have been assigned to 2852 and 2872 cm^{-1} for CH_2 symmetric and CH_2 asymmetric stretching, respectively.[17] The ratio of these peaks indicates the packing density (R) of the lipid membrane.[43] Because there is limited information about the inner membrane (Table 1), MSERS can be used as a method to understand the inner membrane leaflet. In this case, the inner membrane leaflet was induced with small $AuNP_{5nm}$ and confirmed to be located vertically on the membrane by Raman spectroscopy that produced high Raman signals in the fingerprint area than in the hydrocarbon area.

The EF values of AuNP@lipid obtained in this study are listed in Table 3. The EF values at several points (714, 1668, 2852, 2872, and 2930 cm^{-1}), corresponding to $\nu(N-CH_3)$ symmetric, ν(ROH) (from Chol), $\nu(CH_2)$ symmetric, $\nu(CH_2)$ asymmetric (from Chol), and $\nu(CH_3)$ symmetric, respectively,[44,45] are compared. The average EF values of $AuNP_{100nm}$@lipid systems were 94, 56, 111, 121, and 124. The EF values of $AuNP_{5nm}$@lipid systems were relatively higher than those of $AuNP_{100nm}$@lipid systems: the EF values at 714, 1668, 2852, 2872, and 2930 cm^{-1} were 129.3 ± 7.5, 128.2 ± 35.3, 131.3 ± 20.5, 139.4 ± 22.4, and 139.2 ± 21.2, respectively. High concentrations of lipids affected the low uptake of small AuNPs in the inner lipid membrane,[46] which mirrored MSERS signals where the hot spot was not visible in high lipid concentration areas, owing to the proper distance of AuNPs to provide hot spot. In addition, as opposed to supported lipid bilayer systems,[47] this method can be an alternative method to investigate the molecular behaviors on the interior membrane region.

Investigation of Membrane Fluidity and Polarity of AuNP@Lipid. In another viewpoint, we estimated the membrane fluidity and polarity of the lipid membrane of lipid-coated AuNPs. The incorporation of Chol dose dependently decreased the membrane fluidity of the fluid bilayer membranes.[35,38] On this basis, the membrane fluidity and polarity of AuNP@lipid systems were investigated (Figure 4). The results confirmed that the membrane of AuNP@lipid systems was almost similar to DOPC/Chol (60/40) liposome (particle-free lipid bilayer system). Thus, the membrane composition of AuNP@lipid could be DOPC/Chol (60/40), as expected. Compared with the DOPC/Chol liposome as a reference, the membrane properties of AuNP@lipid systems were almost similar to those of liposome systems. Thus, it is assumed that 1-octanethiol hardly disturbs the membrane formation. Herein, DPH and Laurdan were applied to prepared AuNP@lipid systems, and the $1/P$ and GP_{340} values were calculated on previous reports.[35,38] By comparing the difference of membrane properties between AuNP-modified membranes and pure liposomes, it is possible to discuss whether the insertion of AuNPs alters the apparent membrane properties or not.

For $AuNP_{100nm}$@lipid system, the lipid membrane leaflet was attached on the 1-octanethiol-functionalized $AuNP_{100nm}$; thus, a whole membrane area could be influenced by $AuNP_{100nm}$. The results of fluorescent probe studies ($1/P$ and GP_{340}) indicated no significant influence on the modification of $AuNP_{100nm}$. This suggests that the hot spot can be constructed between Chol-enriched domain, and then, the Raman enhancement could be preferentially induced at the Chol-enriched domain. However, $AuNP_{100nm}$@lipid is not suitable for charged membranes because the electrostatic repulsion inhibits the contact between particles (data not shown). Usually, the lipid/probe ratio ≈ 100/1 is employed because the excess amount of fluorescent probes might disturb the membrane properties. In $AuNP_{5nm}$@lipid systems, slight differences of membrane fluidity and polarity could be caused by the insertion of AuNP. It is also notable that the membrane fluidity and polarity are significantly altered by the amount of Chol.[34,35,38] Therefore, possible reasons are that (1) the presence of $AuNP_{5nm}$ slightly made the membrane disordered or that (2) Chol molecules could be accumulated around $AuNP_{5nm}$, and the relative Chol amount in the membrane

Table 3. Summary of Peak Assignments and EF Values for $AuNP_{5nm}$@Lipid and $AuNP_{100nm}$@Lipid Systems

Raman shift [cm^{-1}]	assignment[a]	EF, $AuNP_{100nm}$@lipid[b]	EF, $AuNP_{5nm}$@lipid[c]
714	$\nu_s(N-CH_3)$	94 ± 22.0	129.3 ± 7.5
873	$\nu_a(N-CH_3)$	53.2 ± 27.0	181.4 ± 19.8
1062	$\nu(C-C)_{trans}$	18.4 ± 3.9	68.7 ± 3.0
1087	$\nu(C-C)_{gauche}$	61.2 ± 26.0	63.9 ± 1.8
1126	$\nu(C-C)_{trans}$	25.9 ± 9.9	318.2 ± 8.4
1298	$\tau(CH_2)$	48.9 ± 30.7	116.0 ± 33.9
1442	$\sigma(CH_2)$	77.3 ± 25.8	103.2 ± 27.7
1668	ν(ROH)−Chol	55.7 ± 29.5	128.2 ± 35.3
1738	$\nu(C{=}O)$	90.3 ± 17.9	66.1 ± 10.1
2852	$\nu_s(CH_2)$	111.0 ± 9.0	131.3 ± 20.5
2872	$\nu_a(CH_2)$−Chol	120.9 ± 8.8	139.4 ± 22.4
2930	$\nu_s(CH_3)$	124.4 ± 9.2	139.2 ± 21.2
2960	$\nu_a(CH_3)$	147.7 ± 5.5	149.7 ± 24.7

[a]Cited from the literature.[49−51] [b]Calculated from three reproducible experiments, total lipid concentration was 1 mM. [c]Calculated from three reproducible experiments, total lipid concentration was 0.5 mM.

DOI: 10.1021/acsomega.9b01073
ACS Omega 2019, 4, 13687−13695

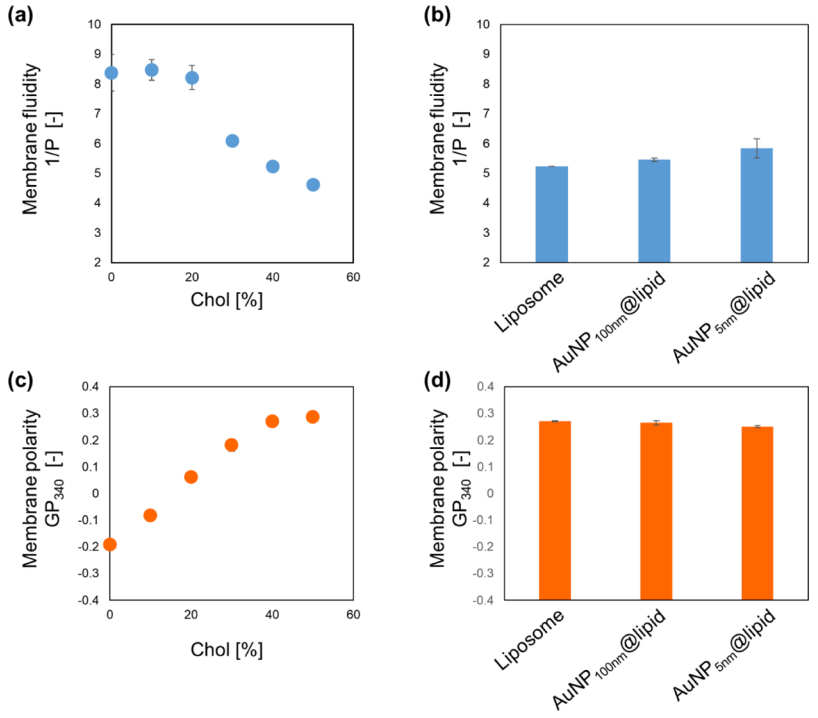

Figure 4. Membrane fluidity and polarity analyses. (a) Relationship of Chol amount and membrane fluidity ($1/P$) in DOPC membranes (liposome systems). (b) Comparison of $1/P$ values. (c) Relationship of Chol amount and membrane polarity (GP_{340}) in DOPC membranes (liposome systems). (d) Comparison of GP_{340} values. Lipid compositions were DOPC/Chol (60/40). All samples were measured at 25 °C. At least three reproducible spectra were obtained for each system. Error bar represents a standard deviation of each data.

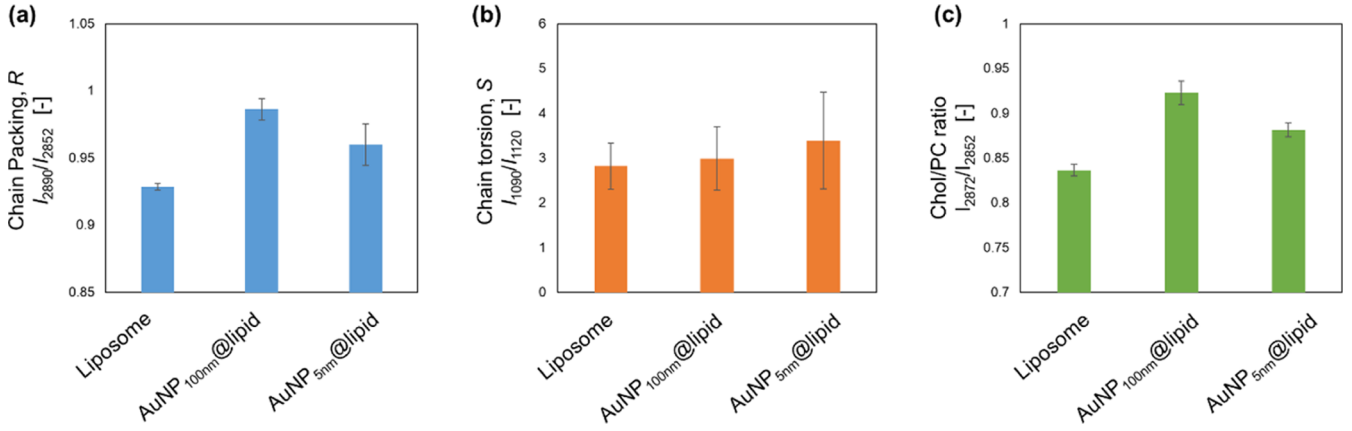

Figure 5. Analyses of lipid membrane properties by Raman. (a) Chain packing, $R = I_{2890}/I_{2852}$. (b) Chain torsion, $S = I_{1090}/I_{1120}$. (c) Chol amount, I_{2872}/I_{2852}. Lipid compositions were DOPC/Chol (60/40). All samples were measured at 25 °C. At least three reproducible spectra were obtained for each system. Error bar represents a standard deviation of each data.

slightly decreased. The membrane can be segregated into DOPC-enriched domain [liquid-disordered phase] and Chol-enriched [liquid-ordered (l_o) phase] domain. It is assumed that $AuNP_{5nm}$ could be interactive with Chol-enriched domain; as a result, the l_o-phase preferred Raman enhancement can be obtained. Although further investigations are needed, the $AuNP_{5nm}$@lipid system is potentially applicable for various systems, including the membranes modified with charged species.

Investigation of Lipid Membrane Properties Based on Raman. In Raman analysis for lipid membranes, both fingerprint (500−2000 cm^{-1}) and C−H stretching regions (2700−3100 cm^{-1}) can be used to know the properties of lipid membranes.[48−51] Because the peaks at 2850 and 2890 cm^{-1} correspond to the symmetric and asymmetric vibrational modes of the $-CH_2-$ group, the peak intensity ratio, $R = I_{2890}/I_{2852}$, is indicative of the hydrocarbon chain packing density.[49] The fingerprint region of the Raman spectrum, in approximately the 1000−1200 cm^{-1} range, is known to be a highly sensitive range for reporting chain−chain interactions (chain torsion: $S = I_{1090}/I_{1120}$).[51] Furthermore, the Chol peak independently appears at 2872 cm^{-1}, and the peak ratio of I_{2872}/I_{2852} reflects the Chol amount in the membrane (see Figure S3). On these bases, the MSERS signals obtained by AuNP@lipid systems are compared with liposome (Figure 5). In common to $AuNP_{100nm}$@lipid, $AuNP_{5nm}$@lipid, and liposome, they resulted in the values of $R < 1$ and $S > 1$, indicating the liquid phase[49] because of the membrane

DOI: 10.1021/acsomega.9b01073
ACS Omega 2019, 4, 13687−13695

composition of DOPC/Chol (60/40). The Chol amount of $AuNP_{5nm}$@lipid seems to be slightly higher than the liposome systems. MSERS of $AuNP_{100nm}$@lipid systems indicated the most ordered membrane properties. This could be due to the location of AuNPs: $AuNP_{5nm}$, which might be accumulated into Chol-enriched domain (i.e., l_o phase). Given that Chol could be heterogeneously distributed in membranes, the hot spot generated in $AuNP_{100nm}$@lipid systems could be a Chol-enriched domain, wherein the membrane is relatively ordered because of enriched Chol.

The Raman intensity of liposome at the total lipid concentration below 10 mM was so weak and usually under the detection limit. Because MSERS measurements were performed at a total concentration below 1 mM, the EF values strongly depend on whether the hot spot is generated or not. The hot spot of $AuNP_{100nm}$@lipid could be induced between the contacted surfaces of $AuNP_{100nm}$@lipid particles, whereas the octanethiol-functionalized $AuNP_{5nm}$ could be incorporated into lipid membranes and then could induce the hot spot inside the membrane. Although further studies are required to investigate the critical reasons for the SERS intensity differences between peaks, the $AuNP_{5nm}$@lipid systems could induce relatively stronger peaks in the finger print regions as compared to $AuNP_{5nm}$@lipid systems. The incorporation of $AuNP_{5nm}$ induced the membrane lipids exiting closely to the AuNPs, which could increase the Raman signals.

CONCLUSIONS

The AuNP-modified DOPC/Chol self-assemblies were prepared to obtain SERS. The Raman signals at the fingerprint region obtained in $AuNP_{5nm}$@lipid systems were slightly stronger than those obtained in $AuNP_{100nm}$@lipid systems. The membrane properties of AuNP@lipid systems and liposomes were compared; in fluorescent probe studies, negligible differences were observed between $AuNP_{100nm}$@lipid and liposome, while the Raman peak intensity analyses suggest the enhanced Chol signals in $AuNP_{100nm}$@lipid. The hot spot of $AuNP_{100nm}$@lipid could be induced between the contacted surfaces of $AuNP_{100nm}$@lipid particles, whereas the octanethiol-functionalized $AuNP_{5nm}$ could be incorporated into lipid membranes and then could induce the hot spot inside the membrane. Considering these results, the $AuNP_{100nm}$@lipid and $AuNP_{5nm}$@lipid systems can be applied to analyze the surface and inner membrane regions, respectively.

This approach will shed lights in characterizing liquid-ordered versus liquid-disordered membrane phases and in detecting the AuNP-associated lipids in membrane systems. Considering the results obtained in this work, slight differences were observed both in fluorescent probe analyses and in SERS. Given an interaction between AuNPs and lipid (or lipid membrane), it can be suggested that (1) $AuNP_{5nm}$ itself disturbs the membrane ordering and (2) the insertion of $AuNP_{5nm}$ altered the distribution of Chol in the membrane. From a relatively stronger Chol signal in $AuNP_{100nm}$@lipid systems, a direct interaction between AuNPs and lipid (especially Chol) should be considered. Although careful studies are required to get more accurate information about AuNP-modified lipid membrane, the SERS method has potential to investigate a wide variety of fractional contents of Chol in membranes and at low lipid/AuNP ratio for a specific application.

ASSOCIATED CONTENT

Supporting Information

The Supporting Information is available free of charge on the ACS Publications website at DOI: 10.1021/acsomega.9b01073.

Size distribution of AuNP; raw spectral data for liposome, $AuNP_{100nm}$@lipid, $AuNP_{5nm}$@lipid, and water; Raman intensity ratio I_{2872}/I_{2852} of DOPC/Chol liposomes; and predicted Chol amount in different $AuNP_{5nm}$@lipid ratios (PDF)

AUTHOR INFORMATION

Corresponding Authors

*E-mail: keishi.suga@cheng.es.osaka-u.ac.jp. Phone: +81-6-6850-6286. Fax: +81-6-6850-6286 (K.S.).

*E-mail: umakoshi@cheng.es.osaka-u.ac.jp. Phone: +81-6-6850-6287. Fax: +81-6-6850-6286 (H.U.).

ORCID

Keishi Suga: 0000-0001-8015-8729

Hiroshi Umakoshi: 0000-0002-9241-853X

Notes

The authors declare no competing financial interest.

ACKNOWLEDGMENTS

This work was primarily supported by the Japan Society for the Promotion of Science (JSPS) KAKENHI Grant-in-Aids for Scientific Research (A) (26249116), Grant-in-Aids for Young Scientists (B) (16K18279), Grant-in-Aids for Challenging Exploratory Research (T15K142040), and Early-Career Scientists (19K15338). The authors express their gratitude for Dr. Haruyuki Ishii (Yamaguchi University) for synthesis of 5 nm AuNP samples. M.F. expresses his gratitude for the Japanese Government (Monbukagakusho: MEXT) scholarship.

REFERENCES

(1) Lyon, L. A.; Peña, D. J.; Natan, M. J. Surface Plasmon Resonance of Au Colloid-Modified Au Films: Particle Size Dependence. *J. Phys. Chem. B* **1999**, *103*, 5826−5831.

(2) Cao, Y. C.; Jin, R.; Mirkin, C. A. Nanoparticles with Raman Spectroscopic Fingerprints for DNA and RNA Detection. *Science* **2002**, *297*, 1536−1540.

(3) Stiles, P. L.; Dieringer, J. A.; Shah, N. C.; Van Duyne, R. P. Surface-enhanced Raman Spectroscopy. *Annu. Rev. Anal. Chem.* **2008**, *1*, 601−626.

(4) Levin, C. S.; Kundu, J.; Janesko, B. G.; Scuseria, G. E.; Raphael, R. M.; Halas, N. J. Interactions of Ibuprofen with Hybrid Lipid Bilayers Probed by Complementary Surface Enhanced Vibrational Spectroscopies. *J. Phys. Chem. B* **2008**, *112*, 14168−14175.

(5) Liu, H.; Wang, H.; Xu, Y.; Guo, R.; Wen, S.; Huang, Y.; Liu, W.; Shen, M.; Zhao, J.; Zhang, G.; Shi, X. Lactobionic Acid-Modified Dendrimer-Entrapped Gold Nanoparticles for Targeted Computed Tomography Imaging of Human Hepatocellular Carcinoma. *ACS Appl. Mater. Interfaces* **2014**, *6*, 6944−6953.

(6) Paciotti, G. F.; Zhao, J.; Cao, S.; Brodie, P. J.; Tamarkin, L.; Huhta, M.; Myer, L. D.; Friedman, J.; Kingston, D. G. I. Synthesis and Evaluation of Paclitaxel-Loaded Gold Nanoparticles for Tumor-Targeted Drug Delivery. *Bioconjugate Chem.* **2016**, *27*, 2646−2657.

(7) Iarossi, M.; Schiattarella, C.; Rea, I.; De Stefano, L.; Fittipaldi, R.; Vecchione, A.; Velotta, R.; Ventura, B. D. Colorimetric Immunosensor by Aggregation of Photochemically Functionalized Gold Nanoparticles. *ACS Omega* **2018**, *3*, 3805−3812.

DOI: 10.1021/acsomega.9b01073
ACS Omega 2019, 4, 13687−13695

(8) Shevach, M.; Fleischer, S.; Shapira, A.; Dvir, T. Gold Nanoparticle-decellularized Matrix Hybrids for Cardiac Tissue Engineering. *Nano Lett.* **2014**, *14*, 5792−5796.
(9) Walde, P.; Umakoshi, H.; Stano, P.; Mavelli, F. Emergent properties arising from the assembly of amphiphiles. Artificial Vesicle Membranes as Reaction Promoters and Regulators. *Chem. Commun.* **2014**, *50*, 10177−10197.
(10) Serrano-Luginbühl, S.; Ruiz-Mirazo, K.; Ostaszewski, R.; Gallou, F.; Walde, P. Soft and Dispersed Interface-rich Aqueous Systems that Promote and Guide Chemical Reactions. *Nat. Rev. Chem.* **2018**, *2*, 306−327.
(11) Grzelczak, M. P.; Danks, S. P.; Klipp, R. C.; Belic, D.; Zaulet, A.; Kunstmann-Olsen, C.; Bradley, D. F.; Tsukuda, T.; Viñas, C.; Teixidor, F.; Abramson, J. J.; Brust, M. Ion Transport Across Biological Membranes by Carborane-Capped Gold Nanoparticles. *ACS Nano* **2017**, *11*, 12492−12499.
(12) Rascol, E.; Devoisselle, J.-M.; Chopineau, J. The Relevance of Membrane Models to Understand Nanoparticles−cell Membrane Interactions. *Nanoscale* **2016**, *8*, 4780−4798.
(13) Contini, C.; Schneemilch, M.; Gaisford, S.; Quirke, N. Nanoparticle−membrane Interactions. *J. Exp. Nanosci.* **2018**, *13*, 62−81.
(14) Tatur, S.; MacCarini, M.; Barker, R.; Nelson, A.; Fragneto, G. Effect of Functionalized Gold Nanoparticles on Floating Lipid Bilayers. *Langmuir* **2013**, *29*, 6606−6614.
(15) Taylor, J.; Huefner, A.; Li, L.; Wingfield, J.; Mahajan, S. Nanoparticles and Intracellular Applications of Surface-enhanced Raman Spectroscopy. *Analyst* **2016**, *141*, 5037−5055.
(16) Czamara, K.; Majzner, K.; Pacia, M. Z.; Kochan, K.; Kaczor, A.; Baranska, M. Raman Spectroscopy of Lipids: A review. *J. Raman Spectrosc.* **2015**, *46*, 4−20.
(17) Movasaghi, Z.; Rehman, S.; Rehman, I. U. Raman Spectroscopy of Biological Tissues. *Appl. Spectrosc. Rev.* **2007**, *42*, 493−541.
(18) Wei, H.; Xu, H. Hot Spots in Different Metal Nanostructures for Plasmon-enhanced Raman Spectroscopy. *Nanoscale* **2013**, *5*, 10794−10805.
(19) Zhang, L.; Granick, S. Lipid Diffusion Compared in Outer and Inner Leaflets of Planar Supported Bilayers. *J. Chem. Phys.* **2005**, *123*, 211104.
(20) Murzyn, K.; Róg, T.; Pasenkiewicz-Gierula, M. Phosphatidylethanolamine-phosphatidylglycerol Bilayer as a Model of the Inner Bacterial Membrane. *Biophys. J.* **2005**, *88*, 1091−1103.
(21) Das, A.; Goldstein, J. L.; Anderson, D. D.; Brown, M. S.; Radhakrishnan, A. Use of Mutant ^{125}I-Perfringolysin O to Probe Transport and Organization of Cholesterol in Membranes of Animal Cells. *Proc. Natl. Acad. Sci. U.S.A.* **2013**, *110*, 10580−10585.
(22) Flanagan, J. J.; Tweten, R. K.; Johnson, A. E.; Heuck, A. P. Cholesterol Exposure at the Membrane Surface is Necessary and Sufficient to Trigger Perfringolysin O Binding. *Biochemistry* **2009**, *48*, 3977−3987.
(23) Maekawa, M.; Fairn, G. D. Complementary Probes Reveal that Phosphatidylserine is Required for the Proper Transbilayer Distribution of Cholesterol. *J. Cell Sci.* **2015**, *128*, 1422−1433.
(24) Sheard, T. M. D.; Hurley, M. E.; Colyer, J.; White, E.; Norman, R.; Pervolaraki, E.; Narayanasamy, K. K.; Hou, Y.; Kirton, H. M.; Yang, Z.; Hunter, L.; Shim, J.; Clowsley, A. H.; Smith, A. J.; Baddeley, D.; Soeller, C.; Colman, M. A.; Jayasinghe, I. Three-dimensional and Chemical Mapping of Intracellular Signaling Nanodomains in Health and Disease with Enhanced Expansion Microscopy. *ACS Nano* **2019**, *13*, 2143−2157.
(25) Bozzuto, G.; Molinari, A. Liposomes as Nanomedical Devices. *Int. J. Nanomed.* **2015**, *10*, 975−999.
(26) Guo, Y.; Terazzi, E.; Seemann, R.; Fleury, J. B.; Baulin, V. A. Direct Proof of Spontaneous Translocation of Lipid-covered Hydrophobic Nanoparticles Through a Phospholipid Bilayer. *Sci. Adv.* **2016**, *2*, No. e1600261.
(27) An, H. H.; Han, W. B.; Kim, Y.; Kim, H.-S.; Oh, Y.; Yoon, C. S. Preparation of SERS Active Ag Nanoparticles Encapsulated by Phospholipids. *J. Raman Spectrosc.* **2014**, *45*, 292−298.
(28) Park, S.-H.; Oh, S.-G.; Mun, J.-Y.; Han, S.-S. Loading of Gold Nanoparticles Inside the DPPC Bilayers of Liposome and their Effects on Membrane Fluidities. *Colloids Surf., B* **2006**, *48*, 112−118.
(29) Rasch, M. R.; Rossinyol, E.; Hueso, J. L.; Goodfellow, B. W.; Arbiol, J.; Korgel, B. A. Hydrophobic Gold Nanoparticle Self-assembly with Phosphatidylcholine Lipid: Membrane-Loaded and Janus Vesicles. *Nano Lett.* **2010**, *10*, 3733−3739.
(30) Suga, K.; Yoshida, T.; Ishii, H.; Okamoto, Y.; Nagao, D.; Konno, M.; Umakoshi, H. Membrane surface-enhanced Raman spectroscopy for sensitive detection of molecular behavior of lipid assemblies. *Anal. Chem.* **2015**, *87*, 4772−4780.
(31) Le Ru, E. C.; Blackie, E.; Meyer, M.; Etchegoin, P. G. Surface Enhanced Raman Scattering Enhancement Factors: A Comprehensive Study. *J. Phys. Chem. C* **2007**, *111*, 13794−13803.
(32) Xu, H.; Aizpurua, J.; Käll, M.; Apell, P. Electromagnetic Contributions to Single-molecule Sensitivity in Surface-enhanced Raman Scattering. *Phys. Rev. E: Stat., Nonlinear, Soft Matter Phys.* **2000**, *62*, 4318−4324.
(33) Lal, S.; Grady, N. K.; Goodrich, G. P.; Halas, N. J. Profiling the Near Field of a Plasmonic Nanoparticle with Raman-based Molecular Rulers. *Nano Lett.* **2006**, *6*, 2338−2343.
(34) De Almeida, R. F. M.; Fedorov, A.; Prieto, M. Sphingomyelin/Phosphatidylcholine/Cholesterol Phase Diagram: Boundaries and Composition of Lipid Rafts. *Biophys. J.* **2003**, *85*, 2406−2416.
(35) Suga, K.; Umakoshi, H. Detection of Nano-sized Sized Ordered Domains in DOPC/DPPC and DOPC/Ch Binary Lipid Mixture Systems of Large Unilamellar Vesicles Using a TEMPO Quenching Method. *Langmuir* **2013**, *29*, 4830−4838.
(36) Niikura, K.; Iyo, N.; Higuchi, T.; Nishio, T.; Jinnai, H.; Fujitani, N.; Ijiro, K. Gold Nanoparticles Coated with Semi-fluorinated Oligo(ethylene glycol) Produce Sub-100 nm Nanoparticle Vesicles without Templates. *J. Am. Chem. Soc.* **2012**, *134*, 7632−7635.
(37) Takayama, M.; Itoh, S.; Nagasaki, T.; Tanimizu, I. A New Enzymatic Method for Determination of Serum Choline-Containing Phospholipids. *Clin. Chim. Acta* **1977**, *79*, 93−98.
(38) Bui, T. T.; Suga, K.; Umakoshi, H. Roles of Sterol Derivatives in Regulating the Membrane Properties of Phospholipid Bilayer Systems. *Langmuir* **2016**, *32*, 6176−6184.
(39) Watanabe, N.; Goto, Y.; Suga, K.; Nyholm, T. K. M.; Slotte, J. P.; Umakoshi, H. Solvatochromic Modeling of Laurdan for Multiple Polarity Analysis of Dihydro-Sphingomyelin Bilayer. *Biphys. J.* **2019**, *116*, 874−883.
(40) Wei, H.; Leng, W.; Song, J.; Willner, M. R.; Marr, L. C.; Zhou, W.; Vikesland, P. J. Improved Quantitative SERS Enabled by Surface Plasmon Enhanced Elastic Light Scattering. *Anal. Chem.* **2018**, *90*, 3227−3237.
(41) Wustholz, K. L.; Henry, A.-I.; McMahon, J. M.; Freeman, R. G.; Valley, N.; Piotti, M. E.; Natan, M. J.; Schatz, G. C.; Van Duyne, R. P. Structure-activity Relationships in Gold Nanoparticle Dimers and Trimers for Surface-enhanced Raman Spectroscopy. *J. Am. Chem. Soc.* **2010**, *132*, 10903−10910.
(42) Sakaguchi, N.; Kimura, Y.; Hirano-Iwata, A.; Ogino, T. Fabrication of Au-Nanoparticle-Embedded Lipid Bilayer Membranes Supported on Solid Substrates. *J. Phys. Chem. B* **2017**, *121*, 4474−4481.
(43) Choe, C.; Lademann, J.; Darvin, M. E. A Depth-dependent Profile of the Lipid Conformation and Lateral Packing Order of the Stratum Corneum in Vivo Measured using Raman Microscopy. *Analyst* **2016**, *141*, 1981−1987.
(44) Brazhe, N. A.; Nikelshparg, E. I.; Prats, C.; Dela, F.; Sosnovtseva, O. Raman Probing of Lipids, Proteins, and Mitochondria in Skeletal Myocytes: A Case Study on Obesity. *J. Raman Spectrosc.* **2017**, *48*, 1158−1165.
(45) Orendorff, C. J.; Ducey, M. W.; Pemberton, J. E. Quantitative Correlation of Raman Spectral Indicators in Determining Conformational Order in Alkyl Chains. *J. Phys. Chem. A* **2002**, *106*, 6991−6998.
(46) Oh, E.; Delehanty, J. B.; Sapsford, K. E.; Susumu, K.; Goswami, R.; Blanco-Canosa, J. B.; Dawson, P. E.; Granek, J.; Shoff, M.; Zhang, Q.; Goering, P. L.; Huston, A.; Medintz, I. L. Cellular Uptake and

DOI: 10.1021/acsomega.9b01073
ACS Omega 2019, 4, 13687−13695

Fate of PEGylated Gold Nanoparticles is Dependent on Both Cell-penetration Peptides and Particle Size. *ACS Nano* **2011**, *5*, 6434−6448.
(47) Mornet, S.; Lambert, O.; Duguet, E.; Brisson, A. The Formation of Supported Lipid Bilayers on Silica Nanoparticles Revealed by Cryoelectron Microscopy. *Nano Lett.* **2005**, *5*, 281−285.
(48) Feng, S.; Chen, R.; Lin, J.; Pan, J.; Chen, G.; Li, Y.; Cheng, M.; Huang, Z.; Chen, J.; Zeng, H. Nasopharyngeal Cancer Detection Based on Blood Plasma Surface-enhanced Raman Spectroscopy and Multivariate Analysis. *Biosens. Bioelectron.* **2010**, *25*, 2414−2419.
(49) Fox, C. B.; Uibel, R. H.; Harris, J. M. Detecting Phase Transitions in Phosphatidylcholine Vesicles by Raman Microscopy and Self-Modeling Curve Resolution. *J. Phys. Chem. B* **2007**, *111*, 11428−11436.
(50) Suga, K.; Otsuka, Y.; Okamoto, Y.; Umakoshi, H. Gel-Phase-like Ordered Membrane Properties Observed in Dispersed Oleic Acid/1-Oleoylglycerol Self-Assemblies: Systematic Characterization Using Raman Spectroscopy and a Laurdan Fluorescent Probe. *Langmuir* **2018**, *34*, 2081−2088.
(51) Batenjany, M. M.; Wang, Z.-Q.; Huang, C.-h.; Levin, I. W. Bilayer Packing Characteristics of Mixed Chain Phospholipid Derivatives: Raman Spectroscopic and Differential Scanning Calorimetric Studies of 1-stearoyl-2-capryl-sn-glycero-3-phosphocholine (C(18): C(10)PC) and 1-stearoyl-2-capryl-sn-glycero-3-phospho-N-trimethylpropanolamine (C(18): C(10)TMPC). *Biochim. Biophys. Acta, Biomembr.* **1994**, *1192*, 205−214.

DOI: 10.1021/acsomega.9b01073
ACS Omega 2019, 4, 13687−13695